Ocean Research 21(2): 87-97, 1999

Circulation in the Southwestern East Sea (Japan Sea) in July 1993 Determined by an Inverse Method

Chang-Woong Shin, Sang-Kyung Byun, Cheolsoo Kim, Young Ho Seung*, and Jae Hak Lee

Physical Oceanography Division, KORDI
Ansan P.O. Box 29, Seoul 425-600, Korea

**Department of Oceanography, Inha University, Inchon 402-751, Korea*

Abstract: To estimate absolute transports by advection in the southwestern East Sea (Japan Sea), an inverse method was applied to CTD data obtained in July 1993. The relative velocities are calculated using the thermal wind equation. The inverse model was formulated to obtain a reference velocity based on the mass conservation in each of four vertical layers within a region enclosed by hydrographic sections and the coastal boundary. The flow patterns in the surface layer are clockwise and anti-clockwise in the regions south and northwest of Ulleung Island, respectively, and a strong northward flow appears in between them. In the second layer, the flow fields are generally weak. The inverse calculation yields the southward flow along the coast, and this suggests that the subsurface low salinity water in the Ulleung Basin is supplied by the southward transport along the east coast of Korea.

Keywords: Inverse method, Reference level, Ulleung Basin, Circulation pattern.

1. Introduction

The Tsushima Warm Current (TWC), which is branched off from the Kuroshio west of Kyushu, carries warm and high salinity water to the East Sea (Moriyasu 1972), and constitutes a main current in the southern part of the East Sea (Japan Sea). The volume transport of the TWC through the western channel of the Korea Strait changes seasonally with its maximum in September (Isobe *et al.* 1994; Yi 1966). The East Korea Warm Current (EKWC) originating from the TWC flows to the north along the eastern coast of Korea. After separating from the coast near 38-40° N, the EKWC forms the polar front with the North Korea Cold Current (NKCC).

Water columns of the southwestern part of the East Sea have been divided into four layers based on the distribution of water masses; the surface water, the TWC water, the East Sea Intermediate Water (ESIW), and the East Sea Proper Water (ESPW). Temperature and salinity of the surface water vary seasonally, and the TWC water has high temperature and high salinity. A layer of salinity minimum and oxygen maximum characterizes the ESIW (Kim and Chung 1984), and the ESPW has nearly homogeneous temperature and salinity. Several studies reported that the ESPW is not a homogeneous single water mass but is composed of different water masses; the Upper portion of Japan Sea Proper Water (UJSPW) (Senjyu and Sudo 1993) or the East Sea Central Water (ESCW), the East Sea Deep Intermediate Water, the East Sea Deep Water, and the East Sea Bottom Water (Kim 1996; Kim *et al.* 1996).

Surface currents of the East Sea have been abundantly studied. However, observations and knowledge of deep currents have not been enough to explain the deep-water circulation (Seung 1992). In 1986, the deep current was measured in water of 840 m depth at the continental slope off the east coast of Korea (Lie *et al.* 1989). Recently, current meters have been deployed to understand the deep circulation in the Japan Basin (Takematsu *et al.* 1999) and in the Ulleung Basin (KORDI 1997).

The direct measurement of deep currents is not an easy task and it is hard to explain the circulation in a large area with only a few measurements. Alternatively, we usually explore the basin-wide circulation pattern based on dynamically calculated geostrophic currents. This approach is convenient, but the geostrophic velocity is still a relative velocity to a reference level. This means that the net volume transport estimated from the geostrophic velocities may not be vanished in a closed area. Wunsch (1978) suggested an inverse method to obtain absolute velocity that satisfies the mass conservation law. Veronis (1987) modified the Wunsch's method to examine the mass transports and circulation patterns in each characteristic layer.

Shin *et al.* (1996) reported that the geostrophic balance holds in the southwestern East Sea. In this study, the inverse method suggested by Veronis (1987) is applied to hydrographic data taken in July 1993 in order to determine absolute velocities in the southwestern part of the East Sea in July 1993. Volume transports are calculated in four layers from the absolute velocities, and the circulation pattern is discussed.

2. Data and Method

Hydrography

Hydrographic data were obtained with a CTD (Neil-Brown Mark IIIB) at 70 stations in the southwestern East Sea by R/V Eardo in July 1993 (Fig. 1). The accuracy of the

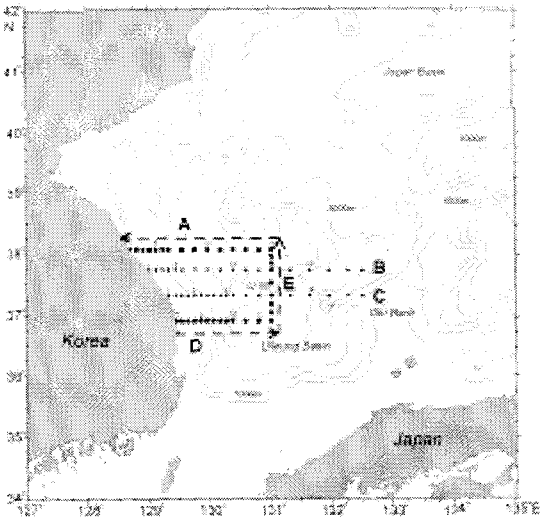

Fig. 1. Observation stations with bottom topography in 500 m intervals. Black circles and rectangles are CTD stations. *U* and *T* mean Ulleung and Tok islands respectively. The inverse method is applied to the region enclosed by observation lines D, E, A and east coast of Korea.

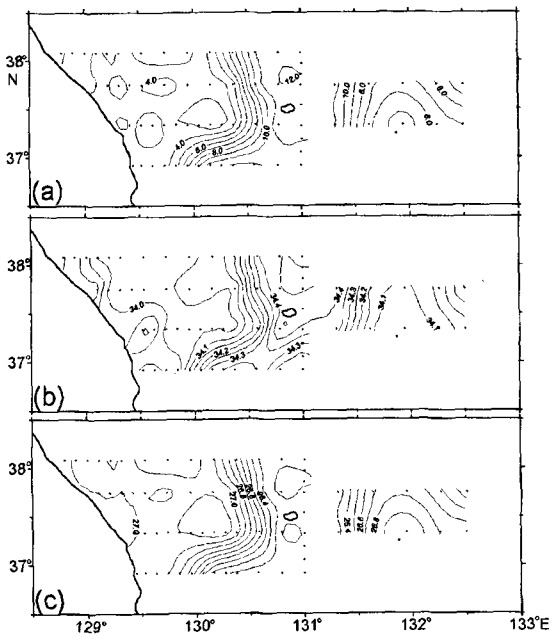

Fig. 2. Horizontal distributions of (a) temperature (°C), (b) salinity (psu) and (c) density (sigma-t) at 100 m depth in July 1993.

CTD is ±0.005°C in temperature and ±0.005 mS·cm^{-1} in conductivity. If the conductivity is 43.0 mS·cm^{-1}, then salinity is 35.0785 psu at 15°C and 0 decibar (db), and the accuracy of salinity is about ±0.0046 psu.

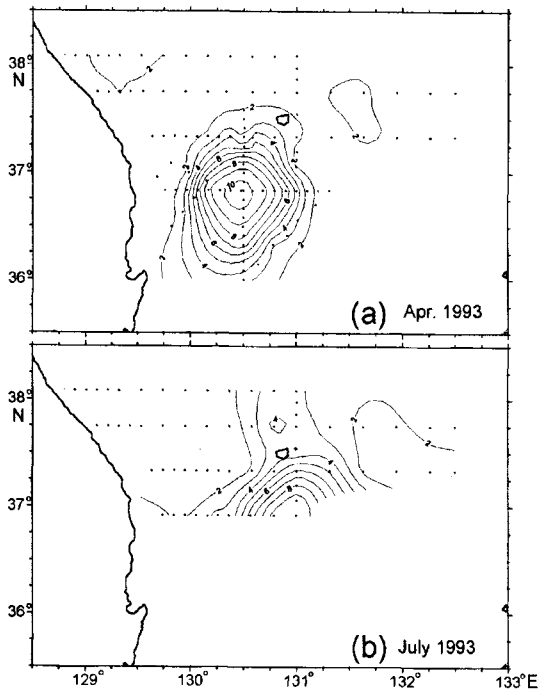

Fig. 3. Horizontal temperature distributions at 200 m depth in (a) April 1993 (after KORDI 1994) and (b) July 1993.

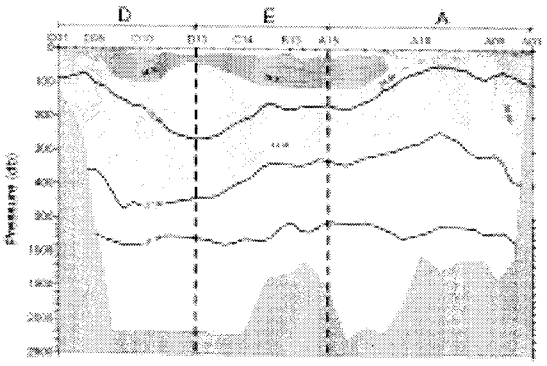

Fig. 4. Vertical section for salinity along lines D, E, and A. Low salinity (<34.06 psu) and high salinity (>34.40 psu) water are hatched and shaded, respectively. Thick solid lines denote potential density surfaces to identify 4 layers. Thick dashed lines divide the observation lines. Note vertical scale for the deeper part than 500 db is larger than shallow part.

Figure 2 shows temperature, salinity and density distributions at 100 m depth. Thermohaline fronts are formed along the inshore part of the EKWC which appears to separate from the east coast south of 37°N and west of 130°E. Salinity is lower than 34.1 psu west of the fronts and higher than 34.3 psu in the other side of the fronts. The thermohaline fronts form a strong contrast of water density with heavier waters inshore of the fronts. The location of the thermal front of 200 m depth differs from that at 100 m depth due to the existence of the Ulleung Warm Eddy (Fig. 3). The eddy, which had a revolution period of 13.6 days, appeared southwest of the Ulleung island in April 1993 (Fig. 3a, Lie *et al.* 1995) and moved to east in July 1993 (Fig. 3b).

The water column is divided into four layers with the characteristic water masses; the surface and TWC waters, the ESIW, the ESCW (or UJSPW), and the deep waters below the ESCW. Figure 4 shows the vertical distribution of salinity along the observation lines D, E and A. High salinity water (shaded area in Fig 4) is shown about 65 km off the coast on line D, while low salinity waters occupy the coastal area of the surface layer. The salinity minimum layer (S <34.06 psu) is shown below the first layer (hatched area in Fig 4), and constitutes mainly the second layer. Figure 5 is the potential temperature-salinity relation for all the data. Warm and saline water (T >12°C, S >34.5 psu) considered as EKWC water shows two salinity maxima at σ_θ=25.5, where the most saline water appears, and at σ_θ=26.0. Shin *et al.* (1998) defined the range of potential density for the ESIW as 26.9-27.3. In this study, the representative σ_θ for the ESIW is considered as 27.1.

We divide the ESPW into two layers. In doing so a careful analysis is required because of its homogeneity. Senjyu and Sudo (1993, 1994) distinguished the UJSPW from the ESPW, and defined the range of σ_θ for the UJSPW as 27.31-27.34 and with σ_θ=27.32 being the representative value at the core of the UJSPW. Based on these studies, σ_θ

=26.9, 27.3, 27.34 are selected as boundary values to identify the four layers (Table 1, Fig. 4).

Table 1. Potential density ranges of the classified layers.

No. of layer	Water mass	Potential density range
1	Surface and Tsushima Warm Current Waters	$\sigma_\theta \leq 26.90$
2	East Sea Intermediate Water	$26.90 < \sigma_\theta \leq 27.30$
3	Upper Portion of Japan Sea Proper Water	$27.30 < \sigma_\theta \leq 27.34$
4	Deep Water	$27.34 < \sigma_\theta$

Empirical Search for Reference Level

Assuming that the fluid flow is hydrostatic and geostrophic, the velocity, v_r at a depth z, relative to a reference depth, z_r is given by

$$v_r = -\frac{g}{fp}\int_{z_r}^{z}\frac{\partial \rho}{\partial x}dz \qquad (1)$$

where g, f and ρ are the acceleration due to gravity, Coriolis parameter, and water density, respectively. The direction of v_r is perpendicular to the x axis. If z_r is chosen, the geostrophic velocity and the advective transport can be calculated from (1).

We further assume that no exchange of water occurs across the layer boundaries, and the flow is steady in the region enclosed by the observation sections (D, E and A) and the coastline (Fig. 1). The net transport for a layer, j, can then be written as

$$Tr_j = \oint\int_{z_{j+1}}^{z_j} \rho v_r \, dz\, ds, \quad 1 \leq j \leq 4 \qquad (2)$$

where z_j and z_{j+1} is the upper and lower boundaries of the jth layer. The horizontal integration is taken along the lines D, E, A and the coastline.

When the geostrophic velocity is calculated at the continental shelf and slope, the initially chosen level of no motion can be deeper than the observation depth. In such a case, if the difference in depth between a station pair is large, the extrapolation of the velocity is needed in a certain depth range near the bottom. In this case, the transports

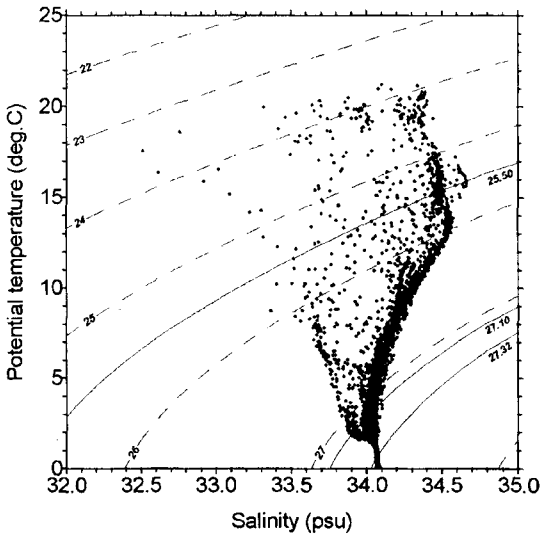

Fig. 5. Potential temperature-salinity relations of CTD data observed in July 1993. The representative potential densities (σ_θ) of the TWC water, the ESIW, and the ESCW are 25.5, 27.1, and 27.32.

depend on the extrapolation method used. The results in turn influence the circulation pattern. In this study, three extrapolation methods are examined:

(i) A vertical shear of the horizontal velocity at a depth of 20 db above the shallower bottom depth in a station pair remains constant from the shallower bottom to 1500 db, which is an approximate mean bottom depth of stations along the observation lines D, E and A.

(ii) The vertical shear decreases linearly from the shallower depth to zero at 1500 db.

(iii) The vertical shear is vanished at depths deeper than the shallower depth in a station pair, i.e., no extrapolation.

It is assumed that the velocity is constant from 1500 db down to the bottom for all cases. To search for the level of no motion (z_r) empirically, the net transport in each layer given by (2) is calculated while changing the reference level from 50 db to the 2500 db at the interval of 50 db. The sum of the squared residuals (ΣTr_j^2) is shown in Fig. 6. ΣTr_j^2 is minimum at 250 db for all cases. And the smallest

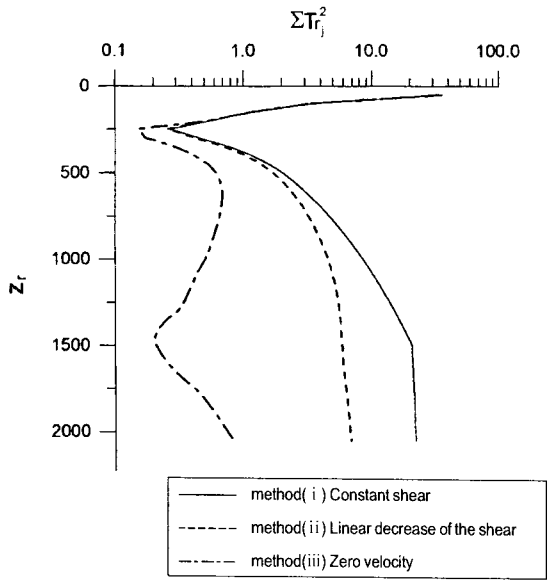

Fig. 6. Total square residual, ΣTr_j^2 (in Sv²), vs. reference pressure, z_r (in decibar), for three extrapolation methods (See text for explanation of the methods). All of the three cases show minimum points at 250 db.

value is obtained with the extrapolation method (iii).

To test the results, two sets of noisy data are generated using a random number generator of L'Ecuyer (Press *et al.* 1992). The maximum differences of temperature, salinity and position between the original and the noisy data are 0.02°C, 0.016 psu and 0.01°(≅1.0 km), respectively. They are larger than the instrument's accuracy of the CTD. The maximum noise of salinity comes from the maximum difference among the data observed at 750 db. ΣTr_j^2 shows its minimum at 250 db both for the original and noisy data regardless of the choice of the extrapolation method (Fig. 7). Here, the difference of the ΣTr_j^2 between the original and the nosy data is considered as a kind of errors which can be caused by the accuracy of the measuring instrument. For case (iii), the errors of ΣTr_j^2 at 250 db are in the range of ±0.0181 Sv² (Sv=10^6 m³/s). The sum of the squared residual (ΣTr_j^2=0.1537 Sv²), however, exceeds the error range (±0.0181 Sv²). The sum of the squared residuals (0.2737, 0.2592 Sv²) for case (i) and (ii) are also over the error ranges (±0.0239, ±0.0228 Sv²). Therefore, the reference level chosen from the empirical search does not satisfy the mass conservation law although the squared residual shows its minimum at 250 db.

Inverse Calculation

To satisfy the mass conservation, it is required to reduce ΣTr_j^2 below a certain value. This means that we must choose an appropriate reference level other than the empirical one. To do this, an inverse method modified by

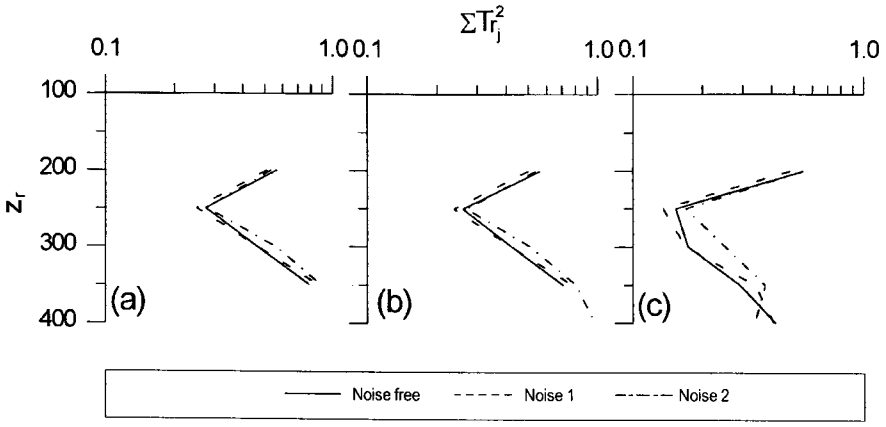

Fig. 7. Total square residual, ΣTr_j^2 (in Sv²), vs. reference pressure, z_r (in decibar), for two noise data sets for the extrapolation methods of (a) method (i), (b) method (ii), and (c) method (iii). For the two noise data sets for the three methods, the ΣTr_j^2 is also minimum at 250 db.

Veronis (1987) was applied to the calculation. The geostrophic current is calculated relative to 250 db. A correction velocity b (x) is then introduced so that v_r+b satisfies the mass conservation for all layers. Then, b can be determined from

$$\oint \int_{z_{j+1}}^{z_j} b dz dx = -Tr_j = c_j, \quad 1 \le j \le 4 \qquad (3)$$

Since the number of stations is discrete, the horizontal integral is approximated by the summation. If the vertical area of the jth layer at a station-pair i is written as a_{ij}, the equation (3) becomes

$$\sum_{i=1}^{34} a_{ij} b_i = c_j, \quad 1 \le j \le 4 \qquad (4)$$

or in matrix notation

$$\mathbf{Ab=c} \qquad (5)$$

where **A**, **b** and **c** are the coefficient matrix, the unknown vector and the data vector, respectively. The inverse model of (5) is strongly underdetermined since the number of unknown variables (i.e. station pairs, n =34) is larger than the number of known data (i.e. layers, m =4). The solution can be obtained by using Singular Value Decomposition (SVD) of matrix **A** with the criterion of the minimum solution length (Press *et al.* 1992). The inverse solution leads to corrections with the minimum mean square amplitude, that is, the minimum correction from the assumed initial state. Thus, the empirical search of the level of no motion is important since it yields a starting point that requires the minimum adjustment. The minimum-norm inverse solution becomes a true minimum (Veronis 1987).

3. Results

Figure 8 shows the vertical distribution of velocity normal to lines D, E, and A determined by the extrapolation method (i) and the inverse method. The level of no motion is different from the empirically found one (250 db). The net transport (ΣTr_j) in each layer, the sum of the squared residuals (ΣTr_j^2) before and after the corrections, and the average of absolute correction velocities are summa-

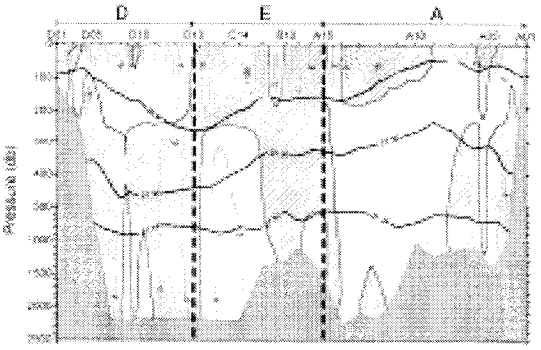

Fig. 8. Vertical section for corrected velocity (cm·s^{-1}) by inverse method along line D, E, and A for the method (i). Positive and negative values indicate inflow and outflow to the closed box area respectively. The levels of no motion (zero velocity lines) are deviated from the initial reference level (250 db) searched experimentally.

Table 2. Comparison between uncorrected and corrected net transport and correction factor for three extrapolation methods.

	(unit)	Tr_1 (m^3·s^{-1})	Tr_2 (m^3·s^{-1})	Tr_3 (m^3·s^{-1})	Tr_4 (m^3·s^{-1})	ΣTr_j^2 (Sv^2)	$\overline{\lvert b \rvert}$ (cm·s^{-1})
Method 1	Uncorrected	285632.6	145956.8	6001.1	-413269.1	0.274	
	Corrected	-3.8	-30.3	-71.2	14.3	0.621×10^{-8}	1.12
Method 2	Uncorrected	271488.7	136627.9	12285.4	-408263.9	0.259	
	Corrected	18.2	6.1	-8.3	-6.4	0.048×10^{-8}	1.11
Method 3	Uncorrected	60456.7	-3573.0	73672.6	-380214.4	0.154	
	Corrected	25.7	57.2	117.1	257.3	8.384×10^{-8}	0.36

rized in Table 2. The corrected value of $\mathrm{T}r_j$ are decreased by 10^{-5}-10^{-2} times as compared to the values without the correction. The extrapolation method (iii) gives the lowest value of

$\Sigma \mathrm{T}r_j^2$ without the correction among the methods, but it gives the largest value after the correction. Method (iii) yields the smallest correction factor, b .

The net transport is approximately zero within the range of error. Thus, the flow paths can be drawn in each layer assuming that the input transport from the outside of the box must flow out to the center of the nearest station pair and the paths do not cross each other. Figure 9 depicts

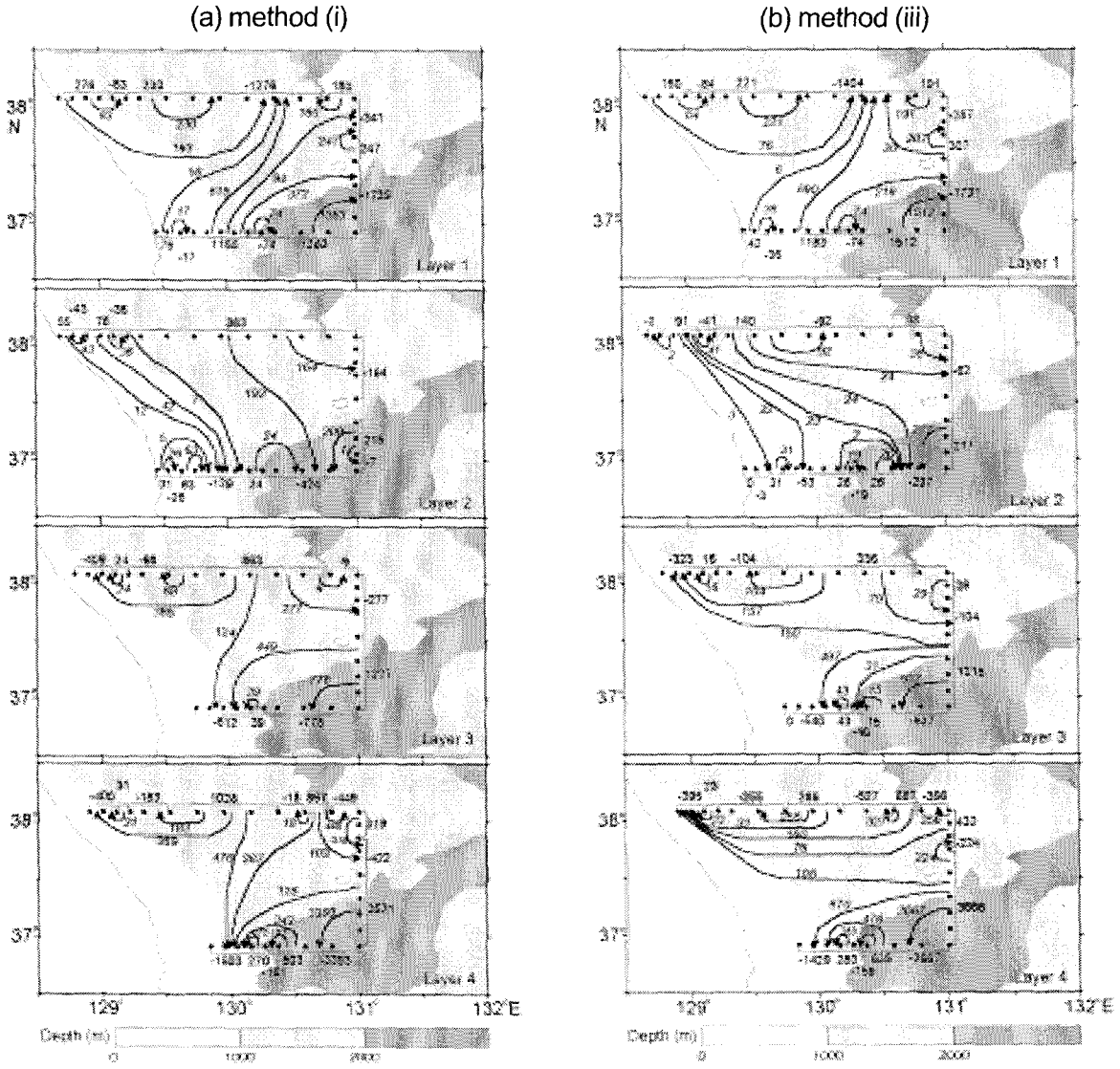

Fig. 9. Transport paths for four layers relative to St. D01 at the southwest corner of the area. Two cases for the extrapolation (a) method (i) and (b) method (iii) are shown here. The four layers have potential density ranges $\sigma_\theta \leq 26.9$, $26.9 \leq \sigma_\theta \leq 27.3$, $27.30 < \sigma_\theta \leq 27.34$, $27.34 <, \sigma_\theta$ respectively. Numbers are transport in 10^{-3} Sv.

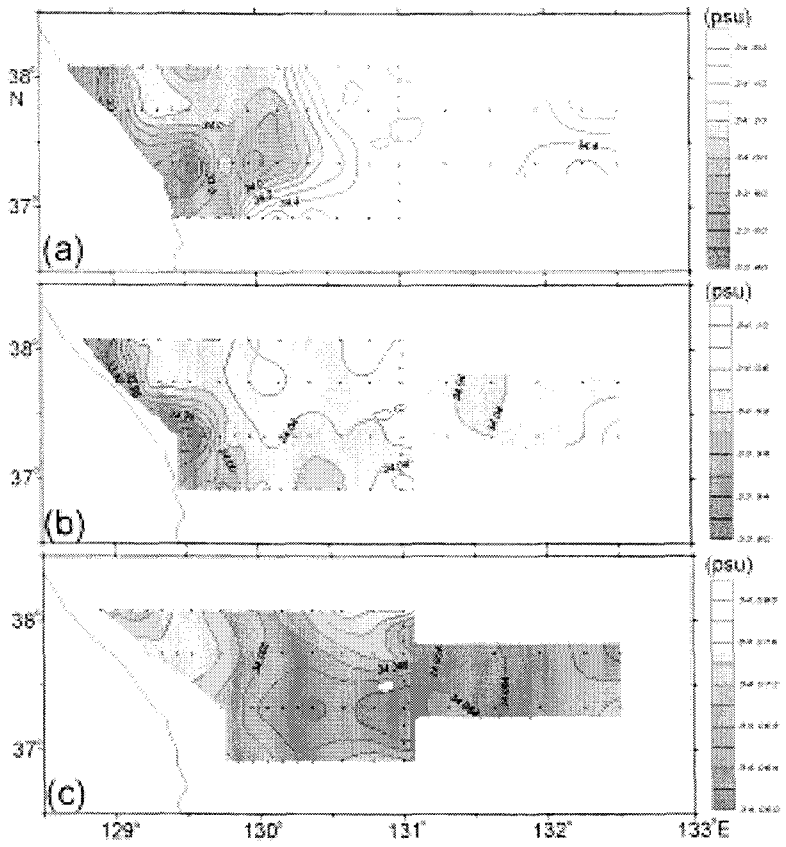

Fig. 10. Distributions of salinity for three isopycnal surface σ_θ=25.5, 27.1, and 27.32. Note the difference in salinity scale.

the flow paths for the extrapolation methods (i) and (iii). The flow paths for the method (ii) are similar to those for the method (i). The flow paths are not unique. Flow patterns, however, are consistent with salinity distributions in each layer shown in Fig. 10 which are prepared on isopycnal surfaces σ_θ=25.5, 27.1 and 27.32 representing the TWC waters, the ESIW, and the ESCW, respectively.

In the first layer, the low salinity water considered as the NKCC flows southward near the east coast of Korea, and flows out northward after turning anti-clockwise (Layer 1 in Fig. 9; Fig. 10 (a)). The high salinity water flows northward and takes two paths in the Ulleung Basin: one in the continental slope region is the EKWC and the other in the basin is a part of the Ulleung Warm Eddy (see Figs. 2, 3, 4). The northward transports of the EKWC and the Ulleung Warm Eddy are estimated to be about 1.2 and 1.4 (method (i)) ~ 1.5 (method (iii)) Sv, respectively. The eastward transport of the warm eddy south of Ulleung Island increases to be about 1.7 Sv after merging with a part of the EKWC water.

In the second layer that is occupied mostly by the ESIW, the transport is smaller than that in the first layer (Layer 2 in Fig. 9; Fig. 10 (b)). However, a remarkable result is that the low salinity water from the east coast of Korea flows into the Ulleung Basin along the continental slope. Below the Ulleung Warm Eddy, the ESIW flows in an anti-clockwise direction and has higher salinity than in other areas.

The third layer that is occupied by the ESCW flows

opposite to the first layer; clockwise in the northwest of Ulleung Island and anti-clockwise in the Ulleung Basin (Layer 3 in Fig. 9). Most of the transports toward the interior region of the Ulleung Basin occur in the southeast of Ulleung Island. On the isopycnal surface (σ_θ=27.32), the salinity distribution also shows low salinity (<34.066 psu) waters intrude into the Ulleung Basin (Fig. 10 (c)).

Flow patterns in the fourth layer are nearly the same as those in the third layer (Layer 4 in Fig. 9). Although the current is slow, the transport is large because of its layer thickness. Southwestward transports of 3.5 (method (i)) ~ 3.6 (method (iii)) Sv occur in the region southeast of Ulleung Island.

4. Discussions and Conclusions

The transport of the EKWC is calculated about 1.2 Sv in the first layer. It is comparable to the transport through the Korea Strait. According to Isobe *et al.* (1994) the volume transport through the Korea Straits was 1.3 Sv in July 1990. Yi (1966) calculated the geostrophic volume transport in the western channel of Korea Straits with an annual average of 0.92 Sv. The previous independently determined results imply that the present inverse calculation is applicable to quantify the currents and transports in the southern East Sea at least in the upper layer.

The inverse calculation shows that the circulation of the lower layer is opposite to the upper layer in the region where the Ulleung Warm Eddy is observed. Na and Kim (1990) conducted laboratory experiments to test the formation of a warm core in the southwestern East Sea. Their major result is that the topography in the western boundary is the most important factor in the formation of a cyclonic motion. They suggest that the cyclonic motion provides the condition for the formation of warm core by lowering the interface. If the Ulleung Warm Eddy is formed by interfacial stresses of the cyclonic motion of lower layer, the opposite circulation would be possible between the upper and the lower layers. However, if the warm eddy is manifestation of the inertial recirculation of the EKWC, it is hard to occur the opposite circulation between layers because the recirculation of the upper layer is stretched downward until it intersects the ocean floor (Greatbatch 1987).

At the continental slope in the mid-east coast of Korea, the result of this study that shows northward transport is not consistent with the southeastward deep current found by Lie *et al.* (1989) from late August to early November 1986. Recently, the trajectory of a PALACE (Profiling Autonomous Lagrangian Circulation Explore) at 700 m depth in the southwestern East Sea shows an anticyclonic circulation (KORDI 1998). The deep circulation and its effects on the upper layer circulation need to be further investigated by means of direct measurements together with indirect methods.

Although the vertical water column is classified into four characteristic layers in this study, it can be divided into many more layers. If that would be the case, the results of inversion could be different from those obtained here. We performed the same calculation with five layers in the vertical by introducing an additional layer with σ_θ=27.342 to the fourth layers, and the result was not different from the case for the four layers in the major flow pattern (not shown here). In the coastal area, some components of the currents such as wind drift and tidal currents can not be resolved by the inverse method.

Three methods were examined to extrapolate velocity from a selected depth to the bottom in the shallow region. The difference in calculated velocity among the methods is little and in the range of 1-2 $cm \cdot s^{-1}$. The reason for the small difference is due to the fact that the distance between adjacent CTD stations is close, and the variation of dynamic height is small because of the homogeneous water mass below the permanent thermocline (Shin *et al.* 1996).

In spite of these problems, conclusions can be drawn on the circulation pattern in the southwestern East Sea deter-

mined from the inversion calculation using the hydrographic data in July 1993. The transports of the EKWC and the Ulleung Warm Eddy are estimated to be 1.2 Sv and 1.4 Sv, respectively. The southeastward current along the continental slope of the east coast of Korea acts to supply the low salinity of the ESIW to the Ulleung Basin. The results also suggest the possibility of the opposite circulation between the surface and the lower layers.

Acknowledgement

The authors give their thanks to the captain and crew of the R/V Eardo as well as the staff of KORDI for their help with the field work. We also thank Dr. J.-Y. Yoon for careful correction of the manuscript and Dr. K.-I. Chang and Dr. Y.-G. Kim for their kind comments.

References

Greatbatch, R. 1987. A model for the inertial recirculation of a gyre. *J. Mar. Res.*, 45, 601-634.

Isobe, A., S. Tawara, A. Kaneko, and M. Kawano. 1994. Seasonal variability in the Tsushiam Warm Current, Tsushiama-Korea Strait. *Continental Shelf Res.*, 14, 23-35.

Kim, K. and J. Y. Chung. 1984. On the salinity-minimum and dissolved oxygen-maximum layer in the East Sea (Sea of Japan). p.55-65. In *Ocean hydrodynamics of the Japan and East China Seas.* ed. by T. Ichiye, Elsevier Science Publisher, Amsterdam.

Kim, K., K.-R. Kim, Y.-G. Kim, Y.-K. Cho, J.-Y. Chung, B.-H. Choi, S.-K. Byun, G.-H. Hong, M. Takematsu. J.-H. Yoon, Y. Volkov, and M. Danchenkov. 1996. New findings from CREAMS observation: water masses and eddies in the East Sea. *J. Korean. Soc. Oceanogr.* 31, 155-163.

Kim, Y.-G.. 1996. A study on the characteristics and circulation of the intermediate and deep layer of the East Sea. Seoul National University Ph.D. Thesis.

KORDI. 1994. A study on the meso-scale warm eddy in the southwestern part of the East Sea. KORDI Rep. BSPN 00222-721-1. (in Korean with English abstract).

KORDI. 1997. Marine environment changes and basin evolution in the East Sea, Korea (I). KORDI Rep. BSPE 97605-00-1037-5. (in Korean with English abstract).

KORDI. 1998. Variability of basin to basin water exchanges in the East Sea. KORDI Rep. BSPE 98710-00-1125-1. (in Korean with English abstract).

Lie, H.-J., M.-S. Suk, and C.-H. Kim. 1989. Observation of southeastward deep currents off the east coast of Korea. *J. Oceanol. Soc. Korea*, 24, 63-68.

Lie, H.-J., S.-K. Byun, I. Bang and C.-H. Cho. 1995. Physical structure of eddies in the southwestern East Sea. *J. Korean Soc. Oceanogr.*, 30, 170-183.

Moriyasu, S. 1972. The Tsushima Current. p.353-369. In *Kuroshio, its physical aspects.* ed. by H. Stommel and K. Yoshida, Univ. of Tokyo Press.

Na, J. Y. and B. H. Kim. 1990. A laboratory study of formation of "the Warm Core" in the East Sea of Korea. *Bull. Korean Fish. Soc.*, 22, 415-423.

Press, W. H., S. A. Teukolsky, W.T. Vetterling, and B.P. Flannery. 1992. Numerical recipes in FORTRAN. Cambridge Univ. Press, Cambridge.

Senjyu, T. and H. Sudo. 1993. Water characteristics and circulation of the upper portion of the Japan Sea Proper Water. *J. Mar. System*, 4, 349-362.

Senjyu, T. and H. Sudo. 1994. The upper portion of the Japan Sea proper water; its source and circulation as deduced from iospycnal analysis. *J. Oceanogr.*, 50, 663-690.

Seung, Y. H. 1992. Water masses and circulations around Korean peninsula. *J. Oceanol. Soc. Korea*, 27, 324-331 (in Korean with English abstract).

Shin, C.-W., S.-K. Byun, and C. Kim. 1996. Comparison between geostrophic currents and measured currents in the southwestern part of the East Sea. *J. Korean Soc.*

Oceanogr., 31, 89-96.

Shin, C.-W., S.-K. Byun, C. Kim, and Y.-H. Seung. 1998. Southward intrusion of the East Sea intermediate water into the Ulleung Basin: observations in 1992 and 1993. *J. Korean Soc. Oceanogr.*, 33, 146-156.

Takematsu, M., Z. Nagano, A. G. Ostrovskii, K. Kim, and Y. Volkov. 1999. Direct measurements of deep currents in the northern Japan Sea. *J. Oceanogr.*, 55, 207-216.

Veronis, G. 1987. Inverse Methods for Ocean Circulation. p. 102-133. In *General circulation of the ocean.* eds. by H. D. I. Abarbanel and W. R. Young. Springer-Verlag, New York.

Wunsch, C. 1978. The general circulation of the North Atlantic west of 50°W determined from inverse methods. *Rev. of Geophys. and Space Physics*, 16, 583-620.

Yi, S.-U. 1966. Seasonal and secular variations of the water volume transport across the Korea Strait. *J. Oceanol. Soc. Korea*, 1, 7-13.

Received Sep. 4, 1999
Accepted Dec. 15, 1999